

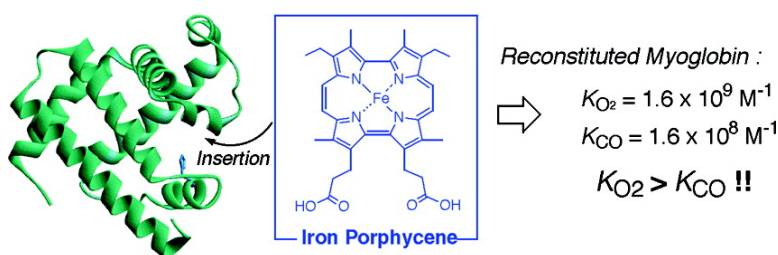
Article

Ligand Binding Properties of Myoglobin Reconstituted with Iron Porphycene: Unusual O Binding Selectivity against CO Binding

Takashi Matsuo, Hirohisa Dejima, Shun Hirota, Dai Murata, Hideaki Sato,
 Takahiro Ikegami, Hiroshi Hori, Yoshio Hisaeda, and Takashi Hayashi

J. Am. Chem. Soc., **2004**, 126 (49), 16007-16017 • DOI: 10.1021/ja045880m • Publication Date (Web): 18 November 2004

Downloaded from <http://pubs.acs.org> on April 5, 2009



More About This Article

Additional resources and features associated with this article are available within the HTML version:

- Supporting Information
- Links to the 1 articles that cite this article, as of the time of this article download
- Access to high resolution figures
- Links to articles and content related to this article
- Copyright permission to reproduce figures and/or text from this article

[View the Full Text HTML](#)

Ligand Binding Properties of Myoglobin Reconstituted with Iron Porphycene: Unusual O₂ Binding Selectivity against CO Binding¹

Takashi Matsuo,^{†,‡} Hirohisa Dejima,[†] Shun Hirota,[§] Dai Murata,[†] Hideaki Sato,^{†,‡} Takahiro Ikegami,[†] Hiroshi Hori,^{||} Yoshio Hisaeda,[†] and Takashi Hayashi^{*,†,‡}

Contribution from the Department of Chemistry and Biochemistry, Graduate School of Engineering, Kyushu University, Fukuoka 812-8581, Japan, PRESTO, Japan Science and Technology Agency (JST), Department of Physical Chemistry, Kyoto Pharmaceutical University, Yamashina, Kyoto 607-8414, Japan, and Division of Bioengineering, Graduate School of Engineering Science, Osaka University, Toyonaka, Osaka 560-8531, Japan

Received July 9, 2004; E-mail: thayatcm@mbox.nc.kyushu-u.ac.jp

Abstract: Sperm whale myoglobin, an oxygen storage hemoprotein, was successfully reconstituted with the iron porphycene having two propionates, 2,7-diethyl-3,6,12,17-tetramethyl-13,16-bis(carboxyethyl)-porphycenatoiron. The physicochemical properties and ligand bindings of the reconstituted myoglobin were investigated. The ferric reconstituted myoglobin shows the remarkable stability against acid denaturation and only a low-spin characteristic in its EPR spectrum. The Fe(III)/Fe(II) redox potential (−190 mV vs NHE) determined by the spectroelectrochemical measurements was much lower than that of the wild-type. These results can be attributed to the strong coordination of His93 to the porphycene iron, which is induced by the nature of the porphycene ring symmetry. The O₂ affinity of the ferrous reconstituted myoglobin is 2600-fold higher than that of the wild-type, mainly due to the decrease in the O₂ dissociation rate, whereas the CO affinity is not so significantly enhanced. As a result, the O₂ affinity of the reconstituted myoglobin exceeds its CO affinity ($M = K_{CO}/K_{O_2} < 1$). The ligand binding studies on H64A mutants support the fact that the slow O₂ dissociation of the reconstituted myoglobin is primarily caused by the stabilization of the Fe–O₂ σ -bonding. The IR spectra for the carbon monoxide (CO) complex of the reconstituted myoglobin suggest several structural and/or electrostatic conformations of the Fe–C–O bond, but this is not directly correlated with the CO dissociation rate. The high O₂ affinity and the unique characteristics of the myoglobin with the iron porphycene indicate that reconstitution with a synthesized heme is a useful method not only to understand the physiological function of myoglobin but also to create a tailor-made function on the protein.

Introduction

Myoglobin (Mb) is a dioxygen (O₂) storage hemoprotein having one protoporphyrin IX iron complex (heme)² **1** as a prosthetic group and plays the role of facilitating O₂ diffusion to mitochondria through the muscle tissue of mammals.³ The heme in Mb is fixed by multiple noncovalent interactions: coordination of His93 to the centered iron, hydrogen bondings of heme propionates with a vicinity of amino acid residues, and hydrophobic contact between peripheral heme alkyl chains and

nonpolar amino acid residues in the heme pocket.^{4,5} O₂ can be reversibly bound on the ferrous heme–iron in Mb, and the hydrogen bonding between the bound O₂ and His64 at the distal site is observed by X-ray crystallography^{6a,b} and neutron diffraction.^{6c} The nature of the Fe–O–O bond has also been discussed based upon the results of resonance Raman,⁷ infrared resonance (IR),^{7,8} and Mössbauer spectroscopic measurements.⁹

[†] Kyushu University.

[‡] PRESTO, JST.

[§] Kyoto Pharmaceutical University.

^{||} Osaka University.

- (1) Abbreviations: Mb, myoglobin; rMb, reconstituted myoglobin; wt-Mb(1), sperm whale wild-type myoglobin; wt-rMb(2), sperm whale reconstituted myoglobin with porphycene **2**; H64A, the mutant whose 64th amino acid residue is replaced with alanine; H64A-Mb(1), sperm whale H64A myoglobin; H64A-rMb(2), sperm whale reconstituted H64A myoglobin with porphycene **2**; hh-Mb(1), horse heart native myoglobin; hh-rMb(2), horse heart reconstituted myoglobin with porphycene **2**; Hb, hemoglobin.
- (2) Strictly speaking, the term “heme” stands for a ferrous porphyrin. As a matter of convenience, we will employ this term throughout this paper for an iron porphyrin in a protein matrix, regardless of its oxidation state.
- (3) *Hemoglobin and Myoglobin in Their Reactions with Ligands*; Antonini, E., Brunori, M., Eds.; North-Holland: Amsterdam, 1971.

- (4) (a) Takano, T. *J. Mol. Biol.* **1977**, *110*, 537–568. (b) Ostermann, A.; Tanaka, I.; Engler, N.; Niimura, F.; Parak, F. G. *Biophys. Chem.* **2002**, *95*, 183–193.
- (5) Hargrove, M. S.; Barrick, D.; Olson, J. S. *Biochemistry* **1996**, *35*, 11293–11299.
- (6) (a) Phillips, S. E. *J. Mol. Biol.* **1980**, *142*, 531–554. (b) Vojtěchovský, J.; Chu, K.; Berendzen, J.; Sweet, R. M.; Schlichting, I. *Biophys. J.* **1999**, *77*, 2153–2174. (c) Phillips, S. E.; Shoenborn, B. P. *Nature* **1981**, *292*, 81–82.
- (7) (a) Barlow, C. H.; Maxwell, J. E.; Wallace, W. J.; Caughey, W. S. *Biochem. Biophys. Res. Commun.* **1973**, *55*, 91–96. (b) Maxwell, J. C.; Volpe, J. A.; Barlow, C. H.; Caughey, W. S. *Biochem. Biophys. Res. Commun.* **1974**, *58*, 166–171.
- (8) (a) Tsubaki, M.; Nagai, K.; Kitagawa, T. *Biochemistry* **1980**, *19*, 379–385. (b) Desbois, A.; Lutz, M.; Banerjee, R. *Biochemistry* **1979**, *18*, 1510–1518. (c) Yu, N.-T.; Benko, B.; Kerr, E. A.; Gersonde, K. *Proc. Natl. Acad. Sci. U.S.A.* **1984**, *81*, 5106–5110. (d) Spiro, T. G. *Iron Porphyrins*; Lever, A. B. P., Gray, H. B., Eds.; Addison Wesley: Reading, MA, 1983; Part II, pp 89–159.
- (9) Parak, B. D. Z. *Naturforsch., C* **1978**, *33*, 488–494.

These measurements revealed that the bond configuration of Fe–O₂ in oxy-Mb is close to that of an Fe(III)–O₂^{•–}-like species.

The kinetic and thermodynamic studies of the ligand binding for Mb have also been done in order to provide useful insights into the physiological property of Mb. Particularly, monitoring the association and dissociation of ligand bindings for a series of Mb mutants directly indicates which amino acid residue significantly modulates the ligand binding process in the protein matrix.¹⁰ According to the ligand binding studies of Mb mutants, the role of His64 is the most crucial. H64X (X = G, A, L, F, and so forth) mutants, in which His64 is replaced with a hydrophobic amino acid, show a drastic acceleration of the O₂ dissociation, leading to the decrease in the O₂ affinity of Mb: $K_{O_2} = 1.1 \times 10^6 \text{ M}^{-1}$ for sperm whale wild-type Mb and $K_{O_2} = 9.0 \times 10^4 \text{ M}^{-1}$ for H64G-Mb at 20 °C and pH 7.0.¹⁰ In addition, the replacement of His64 with Gly causes an increase in the ratio of the CO/O₂ affinities (K_{CO}/K_{O_2} or M' value) to 1700, although the M' value for wild-type Mb is only 25.^{10d} These findings support the fact that His64 undoubtedly stabilizes the heme-bound O₂ via the hydrogen bonding by N^ε–H of the imidazole ring, as indicated in the 3D structure. Such amino acid residues that can form hydrogen bonding with O₂ on the heme are also found in a series of hemoglobins (Hbs).^{10a,11} For example, Hb from *Ascaris suum*, a family of nematodes, has an extremely high O₂ affinity ($K_{O_2} = 3.8 \times 10^8 \text{ M}^{-1}$ at 25 °C)¹² because of the extremely slow O₂ dissociation with the rate constant of 0.004 s^{–1}. In addition, it is noted that the K_{CO}/K_{O_2} value for *Ascaris* Hb is <1, indicating that *Ascaris* Hb selectively binds O₂ against CO. The X-ray analysis and resonance Raman studies for the ferric- and oxy-Hb from the *Ascaris* species have suggested that Gln64 and Tyr30, located in its distal site, provide the systematic hydrogen bonding network with heme-bound O₂ to suppress the O₂ dissociation.¹² The protein has the same prosthetic group, **1**, found in Mb. In this connection, the findings of *Ascaris* Hb with a high O₂ affinity and with an O₂ selectivity against CO have inspired us to improve the physiological function of Mb by protein engineering.¹³

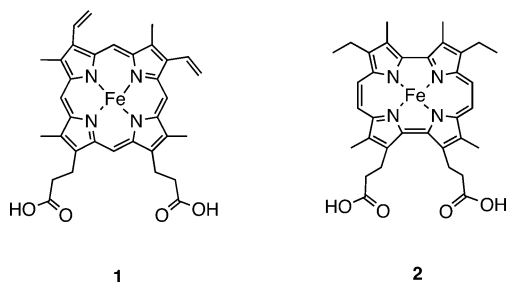
The strategy of modifying Mb can be divided into two approaches: (a) site-directed mutagenesis, and (b) reconstitution using a synthesized prosthetic group.¹⁴ To improve the O₂ affinity of Mb, some research groups have attempted to construct the distal site mimicking that of *Ascaris* Hb by the former method. The L29Y/H64Q sperm whale Mb mutant, however, shows only a 1.6-fold increase in the O₂ affinity, compared to that in wild-type Mb.¹⁵ This is much lower than the O₂ affinity of *Ascaris* Hb. Even in L29Y/H64Q/T67R/I102F, whose structure at the distal site is much closer to that of *Ascaris* Hb,

the enhancement of O₂ affinity is moderate.^{10b} To the best of our knowledge, the Mb mutant with the highest O₂ affinity is L29F/V68F, with the O₂ binding constant of $7.7 \times 10^7 \text{ M}^{-1}$ at 20 °C and pH 7.0.¹⁶ Most of the other mutants prepared so far show an O₂ affinity lower than that in the wild-type.^{10a,16} In contrast, it was reported that the O₂ dissociation rate for sperm whale Mb was successfully diminished by swapping the F-helix of the Mb with that of leghemoglobin.¹⁷ However, the O₂ affinity of the Mb mutant is not as high as that of leghemoglobin because the O₂ association of the mutant is slower than that for leghemoglobin. These findings suggest that it is not always easy to improve the O₂ affinity of Mb by a genetic method.

On the other hand, we have paid attention to another powerful method for modifying the Mb function: replacement of the native heme with an artificially synthesized prosthetic group (“reconstitution”). For the molecular design of a new prosthetic group, three approaches can be pointed out: modifications of the heme propionates,^{18,19} peripheral groups,²⁰ or porphyrin framework.^{21,22} Particularly, it will be of interest to focus on the porphyrin analogues with a different arrangement of the four pyrroles from the C₄-symmetrical porphyrins. Such compounds would be a potent prosthetic group having a drastic influence on the physiological property of Mb because the modification of the ligand framework will alter the electronic and/or structural

- (10) (a) Springer, B. A.; Sligar, S. G.; Olson, J. S.; Phillips, G. N., Jr. *Chem. Rev.* **1994**, *94*, 699–714. (b) Draghi, F.; Miele, A. E.; Travaglini-Allocatelli, C.; Vallone, B.; Brunori, M.; Gibson, Q. H.; Olson, J. S. *J. Biol. Chem.* **2002**, *277*, 7509–7519. (c) Rohlfis, R. J.; Mathews, A. J.; Carver, T. E.; Olson, J. S.; Springer, B. A.; Egeberg, K. D.; Sligar, S. G. *J. Biol. Chem.* **1990**, *265*, 3168–3176. (d) Quillini, M. L.; Arduini, R. M.; Olson, J. S.; Phillips, G. N., Jr. *J. Mol. Biol.* **1993**, *234*, 140–155.
- (11) Mathews, A. J.; Rohlfis, R. J.; Olson, J. S.; Tame, J.; Renaud, J.-P.; Nagai, K. *J. Biol. Chem.* **1989**, *264*, 16573–16583.
- (12) (a) Goldberg, D. E. *Chem. Rev.* **1999**, *99*, 3371–3378. (b) Baere, I. D.; Perutz, M. F.; Kiger, L.; Marden, M. C.; Poyart, C. *Proc. Natl. Acad. Sci. U.S.A.* **1994**, *91*, 1594–1597. (c) Yang, J.; Kloek, A. P.; Goldberg, D. E.; Mathews, F. S. *Proc. Natl. Acad. Sci. U.S.A.* **1995**, *92*, 4224–4228. (d) Peterson, E. S.; Huang, S.; Wang, J.; Miller, L. M.; Vidugiris, G.; Kloek, A. P.; Goldberg, D. E.; Chance, M. R.; Wittenberg, J. B.; Friedman, J. M. *Biochemistry* **1997**, *36*, 13110–13121.
- (13) Other than *Ascaris* Hb, a number of plant and bacterial Hbs with extremely high O₂ affinity have been reported. For example, see: (a) Arredondo-Peter, R.; Hargrove, M. S.; Sarath, G.; Moran, J. F.; Lohman, J.; Olson, J. S. *Plant Physiol.* **1997**, *115*, 1259–1266. (b) Trevasis, B.; Watts, R. A.; Andersson, C. R.; Llewellyn, D.; Hargrove, M. S.; Olson, J. S.; Dennis, E. S.; Peacock, W. J. *Proc. Natl. Acad. Sci. U.S.A.* **1997**, *94*, 12230–12234. (c) Duff, S. M. G.; Wittenberg, J. B.; Hill, R. D. *J. Biol. Chem.* **1997**, *272*, 16746–16752. (d) Kiger, L.; Rashid, A. K.; Griffon, N.; Haque, M.; Moens, L.; Gibson, Q. H.; Poyart, C.; Marden, M. C. *Biophys. J.* **1998**, *75*, 990–998. (e) Couture, M.; Das, T. K.; Lee, H. C.; Peisach, J.; Rousseau, D. L.; Wittenberg, B. A.; Wittenberg, J. B.; Guertin, M. J. *Biol. Chem.* **1999**, *274*, 6898–6910. (f) Dewilde, S.; Kiger, L.; Burnester, T.; Hankeln, T.; Baudin-Creux, V.; Aerts, T.; Marden, M. C.; Caubergs, R.; Moens, L. J. *Biol. Chem.* **2001**, *276*, 38949–38955. (g) Hunt, P. W.; Klok, E. J.; Trevasis, B.; Watts, R. A.; Ellis, M. H.; Peacock, W. J.; Dennis, E. S. *Proc. Natl. Acad. Sci. U.S.A.* **2002**, *99*, 17197–17202. (h) Kundu, S.; Trent, J. T., III; Hargrove, M. S. *Trends Plant Sci.* **2003**, *8*, 387–393.
- (14) Hayashi, T.; Hisaeda, Y. *Acc. Chem. Res.* **2002**, *35*, 35–43.
- (15) Travaglini-Allocatelli, C.; Cutruzzola, F.; Brancaccio, A.; Vallone, B.; Brunori, M. *FEBS Lett.* **1994**, *352*, 63–66 (Erratum: *FEBS Lett.* **1994**, *356*, 151).
- (16) Dou, Y.; Mailllet, D. H.; Eich, R. F.; Olson, J. S. *Biophys. J.* **2002**, *98*, 127–148.
- (17) Kundu, S.; Snyder, B.; Das, K.; Chowdhury, P.; Park, J.; Petrich, J. W.; Hargrove, M. S. *Proteins* **2002**, *46*, 268–277.
- (18) (a) Hayashi, T.; Hitomi, Y.; Ogoshi, H. *J. Am. Chem. Soc.* **1998**, *120*, 4910–4915. (b) Heleg-Shabtai, V.; Gabriel, T.; Willner, I. *J. Am. Chem. Soc.* **1999**, *121*, 3220–3221. (c) Hamachi, I.; Shinkai, S. *Eur. J. Org. Chem.* **1999**, 539–549. (d) Matsuo, T.; Hayashi, T.; Hisaeda, Y. *J. Am. Chem. Soc.* **2002**, *124*, 11235–11236. (e) Sato, H.; Hayashi, T.; Ando, T.; Hisaeda, Y.; Ueno, T.; Watanabe, Y. *J. Am. Chem. Soc.* **2004**, *126*, 436–437.
- (19) (a) DiNello, R. K.; Dolphin, D. H. *J. Biol. Chem.* **1981**, *256*, 6903–6912. (b) Hauksson, J. B.; La Mar, G. N.; Pandey, R. K.; Rezzano, I. N.; Smith, K. M. *J. Am. Chem. Soc.* **1990**, *112*, 8315–8323. (c) Hunter, C. L.; Lloyd, E.; Eltis, L. D.; Rafferty, S. P.; Lee, H.; Smith, M.; Mauk, A. G. *Biochemistry* **1997**, *36*, 1010–1017. (d) Hayashi, T.; Matsuo, T.; Hitomi, Y.; Okawa, K.; Suzuki, A.; Shiro, Y.; Iizuka, T.; Hisaeda, Y.; Ogoshi, H. *J. Inorg. Chem.* **2002**, *91*, 94–100.
- (20) (a) Sono, M.; Asakura, T. *J. Biol. Chem.* **1975**, *250*, 5227–5232. (b) Chang, C. K.; Ward, B.; Ebina, S. *Arch. Biochem. Biophys.* **1984**, *231*, 366–371.
- (21) (a) Stynes, D. V.; Liu, S.; Marcus, H. *Inorg. Chem.* **1985**, *24*, 4335–4338. (b) Christopher, F., Jr.; Takimura, T.; Sessler, J. L. *Abstracts of Papers*; 213th ACS National Meeting, San Francisco, CA; American Chemical Society: Washington, DC, 1997; INOR-519. (c) Neya, S.; Hori, H.; Imai, K.; Kawamura-Konishi, Y.; Suzuki, H.; Shiro, Y.; Iizuka, T.; Funasaki, N. *J. Biochem.* **1997**, *121*, 654–660. (d) Sotiriou-Leventis, C.; Chang, C. K. *Inorg. Chim. Acta* **2000**, *311*, 113–118. (e) Neya, S.; Imai, K.; Hori, H.; Ishikawa, H.; Ishimori, K.; Okuno, D.; Nagatomo, S.; Hoshino, T.; Hata, M.; Funasaki, N. *Inorg. Chem.* **2003**, *42*, 1456–1461.
- (22) The employment of a non-tetrapyrrole prosthetic group has also been reported. (a) Kieldahl, N. K.; Kolis, J. W.; Beckett, J.; Holland, G. F.; Patz, M. A. *J. Coord. Chem.* **1983**, *12*, 259–272. (b) Ohashi, M.; Koshiyama, T.; Ueno, T.; Yanase, M.; Fujii, H.; Watanabe, Y. *Angew. Chem., Int. Ed.* **2003**, *42*, 1005–1008.

Chart 1



properties of the coordinated iron atom. In fact, there have been several trials to obtain a special Mb with a high O₂ affinity, where iron phthalocyanine,^{21a} azahemin,^{21b} iron corphycene,^{21c} iron chlorin,^{21d} hemiporphycene,^{21e} and so forth, were used as an artificial prosthetic group. These compounds, however, have revealed moderate or negative effects on the O₂ affinity of Mb. In contrast, to address the utility of the reconstitutive method for modulating the property of Mb, we have focused on an iron porphycene as a new prosthetic group. Porphycene is one of the tetrapyrrolic porphyrin isomers and was first synthesized by Vogel and co-workers in 1986,²³ where two bipyrroles were linked with two ethylene bridges (such as **2** in Chart 1). The various spectroscopic and structural studies have shown that the structural nature of porphycenes and metalloporphycenes gives rise to quite different physicochemical properties from that observed in the corresponding porphyrins, mainly because the geometry of the four pyrroles in porphycene leads to a lower symmetry of the framework than that in porphyrin ($D_{4h} \rightarrow D_{2h}$).^{23–29} These characteristics suggest that the reconstitution of Mb with an iron porphycene would be a useful method to enhance the O₂ affinity of Mb because the change in the energy levels of d-orbitals and/or the coordination behavior of an axial ligand effectively regenerates the O₂ affinity of the iron in tetrapyrroles.^{30–32}

In a previous report, we demonstrated that horse heart Mb reconstituted with porphycene **2** (hh-rMb(**2**)) showed an O₂ affinity 1400-fold higher than that of the native Mb (hh-Mb(**1**)) (rMb is reconstituted Mb).³³ However, it has not been clear why

the replacement of the native heme with porphycene **2** drastically enhances the O₂ affinity of Mb. Furthermore, the CO affinity, another important property of the ligand binding in Mb, was not reported. In this paper, we demonstrate some of the physicochemical properties of sperm whale rMb(**2**), wt-rMb(**2**), and discuss the fashions of ligand binding for the deoxy-rMb(**2**), based upon a series of kinetic parameters for both O₂ and CO bindings. The rMb(**2**) prepared in this study also has a remarkably high O₂ affinity. Surprisingly, wt-rMb(**2**) shows the characteristic O₂/CO discrimination, where its O₂ affinity exceeds its CO affinity. The spectroscopic analyses for wt-rMb(**2**) indicated that the high O₂ affinity is attributed to the nature of the porphycene ring employed as a prosthetic group. Furthermore, porphycene **2** was incorporated into the apo-H64A-Mb to clarify the contribution of the hydrogen bonding between the amino acid residues and the bound O₂ to the stability of the oxygenated wt-rMb(**2**). Throughout this study, we wish to propose that an iron porphycene is superior to the native heme as a prosthetic group in order to stabilize the oxygenated iron complex in Mb.

Experimental Section

Instruments. The UV–vis spectra were recorded on a Hitachi U-3210 double-beam spectrometer. The mass analysis of a reconstituted Mb was carried out using a TOF mass spectrometer equipped with electrospray ionization on an Applied Biosystems Mariner API-TOF workstation. The pH values were monitored by a Beckman Φ 71 pH meter. The spectroelectrochemical measurement was performed by regulating the potentials using a Hokuto Denko HA-305 potentiostat/galvanostat. The EPR spectra were measured by a Varian E-12 spectrometer equipped with an Oxford ESR-900 liquid helium cryostat. The IR spectra of the CO-ligated Mbs were measured using a JASCO FT/IR-620 spectrometer. Kinetic measurements for the ligand binding were carried out with a stopped-flow/laser flash photolysis system constructed by Unisoku Co., Ltd. (Osaka, Japan). A Xe Arc lamp was employed as a source of the probe light to follow the spectral changes. For laser flash photolysis, a sample was excited with 5 ns pulses (532 nm) from a Q-switched Nd:YAG laser (Surelite I, Continuum).

Materials. All reagents and chemicals were obtained from commercial sources and used as received unless otherwise noted. Porphycene **2** was synthesized by the method described in a previous paper.³³ The sperm whale wild-type and H64A Mbs were expressed in *Escherichia coli*. These Mbs were purified by column chromatography through CM-52 (Whatman) and Sephadex G-25 (Amersham Biosciences) columns. O₂, N₂ (purity > 99.999%), and CO (purity > 99.995%) were purchased from Sumitomo Seika Chemicals Co., Ltd.

Preparation of Myoglobins Reconstituted with Porphycene 2, rMb(2**s).** Apomyoglobin (apo-Mb) was prepared from met-Mb by Teale's 2-butanone method.³⁴ A solution of **2** (buffer/pyridine or buffer/DMSO = 1/1) was added to a solution of apo-Mb and was slowly shook at 4 °C. The solution was then dialyzed against a 100-fold volume of 100 mM phosphate buffer (pH 7.0, 3 h \times 3, at 4 °C). After the mixture was centrifuged (4000 rpm, 10 min, at 2 °C) and concentrated, the solution was passed through a Sephadex G-25 column. The solution of a purified rMb(**2**) was concentrated and maintained at 4 °C. The protein solution was used within 2 days.

Acid Titration. To 3 mL of a 100 mM KCl solution was added 10 μ L of a concentrated Mb solution (~0.4 mM) in 100 mM phosphate buffer (pH 7.0). The UV–vis spectrum and pH value of the Mb solution

- (23) Vogel, E.; Köcher, M.; Schmickler, H.; Lex, J. *Angew. Chem., Int. Ed.* **1986**, *25*, 257–259.
- (24) Sessler, J. L.; Gebauer, A.; Vogel, E. In *The Porphyrin Handbook*; Kadish, K. M., Smith, K. M., Guillard, R., Eds.; Academic Press: San Diego, CA, 2000; Vol. 2, Chapter 8, pp 1–52 and references therein.
- (25) Ohgo, Y.; Neva, S.; Ikeue, T.; Takahashi, M.; Takeda, M.; Funasaki, N.; Nakamura, M. *Inorg. Chem.* **2002**, *41*, 4627–4629.
- (26) Rachlewicz, K.; Latos-Grażyński, L.; Vogel, E.; Ciunik, Z.; Jerzykiewicz, L. B. *Inorg. Chem.* **2002**, *41*, 1979–1988.
- (27) Bernard, C.; Le Mest, Y.; Gisselbrecht, J. P. *Inorg. Chem.* **1998**, *37*, 181–190.
- (28) (a) D'sauza, F.; Boulas, P.; Aukauloo, A. M.; Guillard, R.; Kisters, M.; Vogel, E.; Kadish, K. M. *J. Phys. Chem.* **1994**, *98*, 11885–11891. (b) Gisselbrecht, J. P.; Gross, M. *J. Am. Chem. Soc.* **1990**, *112*, 8618–8620. (c) Ranner, M. W.; Forman, A.; Wu, W.; Chang, C. K.; Fajer, J. *J. Am. Chem. Soc.* **1989**, *111*, 8618–8621. (d) Oertling, W. A.; Wu, W.; López-Garriga, J. J.; Kim, Y.; Chang, C. K. *J. Am. Chem. Soc.* **1991**, *113*, 127–134. (e) Kadish, K. M.; Tabard, A.; Caemelbecke, E. V.; Aukauloo, A. M.; Richard, P.; Guillard, R. *Inorg. Chem.* **1998**, *37*, 6168–6175. (f) Bernard, C.; Gisselbrecht, J. P.; Gross, M.; Vogel, E.; Lausmann, M. *Inorg. Chem.* **1994**, *33*, 2393–2401.
- (29) (a) Hayashi, T.; Nakashima, Y.; Ito, K.; Ikegami, T.; Aritome, I.; Aoyagi, K.; Ando, T.; Hisaeda, Y. *Inorg. Chem.* **2003**, *42*, 7345–7347. (b) Hayashi, T.; Nakashima, Y.; Ito, K.; Ikegami, T.; Aritome, I.; Suzuki, A.; Hisaeda, Y. *Org. Lett.* **2003**, *5*, 2845–2848.
- (30) Momenteau, M.; Reed, C. A. *Chem. Rev.* **1994**, *94*, 659–698 and references therein.
- (31) Chang, C. K.; Traylor, T. G. *J. Am. Chem. Soc.* **1973**, *95*, 8477–8479.
- (32) Collman, J. P.; Bauman, J. I.; Doxsee, K. M.; Sessler, J. L.; Morris, R. M.; Gibson, Q. H. *Inorg. Chem.* **1983**, *22*, 1427–1432.

(33) Hayashi, T.; Dejima, H.; Matsuo, T.; Sato, H.; Murata, D.; Hisaeda, Y. *J. Am. Chem. Soc.* **2002**, *124*, 11226–11227.

(34) (a) Teale, F. W. *Biochim. Biophys. Acta* **1959**, *35*, 543. (b) Yonetani, T.; Asakura, T. *J. Biol. Chem.* **1969**, *244*, 4580–4588.

were monitored for each addition of 10 μL of 100 mM HCl at 25 $^{\circ}\text{C}$. The $\text{p}K_{1/2}$ value, the pH corresponding to a 50% loss of a prosthetic group, was determined by fitting the titration curve to the modified Henderson–Hasselbach equation.³⁵

EPR Measurement. EPR measurements were carried out at the X-band (9.35 GHz) microwave frequency with 100 kHz field modulation (0.5 mT) at 15 K. The range of the microwave power is 5 mW. The sample concentration was $\sim 400 \mu\text{M}$, and the volume was 50 μL .

Determination of Fe(III)/Fe(II) Redox Potential. The spectroelectrochemical measurement was performed using the modified method described in a previous report.³⁶ The measurement was carried out at 25 $^{\circ}\text{C}$ under a N_2 atmosphere with an optically transparent thin-layer electrode cell ($L = 0.5 \text{ mm}$). A working electrode and a counter electrode made of Pt mesh were employed along with an Ag/AgCl reference electrode. Anthraquinone-2-sulfonate ($E = -230 \text{ mV}$ vs NHE) was employed as the electron mediator. The data obtained were fitted to a Nernst equation, and the resulting midpoint of the Fe(III)/Fe(II) redox potential was corrected to the value referenced to NHE.

Preparation of O₂- and CO-Ligated Myoglobins, MbO₂s and MbCOs. To prepare oxygenated Mbs (MbO₂s), except for the H64A-MbO₂s, the met-Mbs were reduced by sodium dithionite to give deoxy-Mbs and separated from excess sodium dithionite by Sephadex G-25 gel filtration with 100 mM phosphate buffer, pH 7.0. During the elution, the deoxy-Mb species smoothly changed to the MbO₂ by dissolving O₂ in the buffer. The CO forms of Mbs (MbCOs) were obtained by reduction with a slight excess of sodium dithionite under a CO atmosphere. For the measurements of the CO dissociation from MbCOs, excess dithionite was removed by the Sephadex G-25 gel filtration with elution of CO-saturated 100 mM phosphate buffer, pH 7.0.

Kinetic Measurement for Ligand Bindings. Kinetic studies were carried out in 100 mM phosphate buffer, pH 7.0, at 25 $^{\circ}\text{C}$, except for monitoring the autoxidation rate at 37 $^{\circ}\text{C}$. The O₂ associations for wt-Mb(1) and wt-rMb(2) were measured by following the changes in the absorbance at 435 nm for wt-Mb(1) or at 619 nm for wt-rMb(2) after excitation of a MbO₂ by laser flash photolysis ($\lambda_{\text{ex}} = 532 \text{ nm}$, 5 ns pulse) under atmospheric pressure in air. For H64A-Mb(1), the O₂-saturated buffer at 4 $^{\circ}\text{C}$ was employed for the Sephadex G-25 gel filtration after being reduced with dithionite. After the obtained oxy form was directly injected from the gel column into an optical cell under the O₂ atmosphere, the O₂ association was observed by following the absorbance change at 435 nm by laser flash photolysis. For H64A-rMb(2), the CO-bound form, equilibrated with the atmosphere of CO/O₂ = 5/95, was excited by laser flash, and the absorbance change at 365 nm during the initial stage was followed.³⁷ The first-order rate constant was determined by fitting the reaction curve by a nonlinear least-squares method. Dividing the rate constants by the concentration of O₂ under each measurement condition afforded the rate constants of the O₂ associations. The probe light used to follow the kinetics was passed through a monochromator.

The O₂ dissociations were measured by displacement with CO or the ferricyanide method by a stopped-flow apparatus. For the MbO₂s, except for the mutants, the ferricyanide method was employed. Under $[\text{K}_3\text{Fe}(\text{CN})_6] \gg [\text{Mb}]$, the decay of the absorbance at 580 nm for wt-Mb(1) or at 619 nm for wt-rMb(2) was analyzed by a first-order rate law. The probe light used to follow the kinetics was passed through a monochromator. The observed rate constants leveled off for a huge excess of $\text{K}_3\text{Fe}(\text{CN})_6$ to yield the dissociation rate constant. In the case of the mutant Mbs, H64A-Mb(1) and H64A-rMb(2), a better-devised procedure was needed due to their extremely rapid autoxidations. A deoxy mutant Mb was prepared in a glovebox ($< 1 \text{ ppm O}_2$) and loaded on a double-mixing stopped-flow apparatus without air contact. The

deoxy-Mb was first mixed with O₂-saturated buffer to yield the oxy form. After an aging time of 1.0 s, the solution was further mixed with CO-saturated buffer. The spectral changes in the range of 380–410 nm were monitored after the second mixing. The probe light at a shorter wavelength ($< 360 \text{ nm}$) was cut off with an optical filter (Sigma Koki Co., Ltd., Japan). With an excess of a ligand, the observed rate constant, k_{obs} , is determined as follows:^{10c}

$$k_{\text{obs}} = k_{\text{off}(\text{O}_2)} / (1 + k_{\text{on}(\text{O}_2)}[\text{O}_2] / k_{\text{on}(\text{CO})}[\text{CO}])$$

Autoxidations for the MbO₂s were measured by following the spectral changes in the range of 500–700 nm every 15 min at 37 $^{\circ}\text{C}$. The time course of absorbance at 580 nm for wt-Mb(1) or at 619 nm for wt-rMb(2) was analyzed by first-order kinetics to afford the autoxidation rate. For H64A-Mb(1) and H64A-rMb(2), a deoxy-Mb prepared in a glovebox was mixed with 40% O₂-saturated to follow the spectral changes in the range of 500–700 nm. The shorter wavelength component ($< 400 \text{ nm}$) in the probe light was cut off with an optical filter.

The CO associations were measured by monitoring the changes in the absorbance at 425 nm for wt-Mb(1) and H64A-Mb(1) or at 613 nm for wt-rMb(2) and H64A-rMb(2) after excitation by laser flash photolysis under 1 atm of CO. For the measurements, the probe light at the shorter wavelength ($< 400 \text{ nm}$) was cut off.

The CO dissociations from the CO-ligated Mbs were measured by displacement with O₂ for wt-rMb(2) or NO for the others. A solution of a MbCO was mixed with O₂- or NO-saturated buffer by a stopped-flow apparatus, and the decrease in absorbance at 423 nm for wt-Mb(1) and H64A-Mb(1) or 613 nm for wt-rMb(2) and H64A-rMb(2) was monitored.

IR Measurement for Carbon Monoxide Myoglobins. The C–O stretching modes, $\nu(\text{C–O})$, in the MbCOs were measured in a cell ($L = 0.1 \text{ mm}$) with CaF₂ windows. The measurement was carried out at room temperature, and the background spectrum was collected for the corresponding deoxy-Mb.

Results

Characterization of Reconstituted Myoglobin. The rMb with iron porphycene **2** was successfully obtained by a conventional method adapted for the incorporation of an iron porphyrin into apo-Mb. The color of the solution turned from green to blue upon the reconstitution due to the increase in the absorbance at 624 nm. After the purification by chromatography, the blue fraction of $M_w > 10\,000$ was characterized by ESI-TOF mass spectroscopy. The mass spectrum of the fraction recorded under neutral conditions (in 10 mM AcONH₄) displays a series of protein ions in charge states ranging from 7+ to 13+, as shown in Figure 1. The deconvoluted spectrum gave the mass number at 17 950, which corresponds to the mass number of apo-Mb from sperm whale and that of **2**. Therefore, the component was identified as wt-rMb(2).

The UV–vis spectrum of met-wt-rMb(2) showed three characteristic bands at 387, 563, and 624 nm, as depicted in Figure 2. Particularly, the band observed at 563 nm suggests the axial coordination to the iron porphycene because there is no characteristic band in the 550–600 nm region for **2**–Cl without an imidazole ligand.^{27,28d} There is no significant difference in the peak positions among the rMbs from the sperm whale, horse heart, and H64A mutant.

An increase in the pH value of a met-wt-rMb(2) solution leads to a blue shift in the characteristic band at 620–624 nm. This finding suggests that a water molecule weakly binding to the iron is deprotonated to the hydroxide in the alkaline pH region.

- (35) Lloyd, E.; Burk, D. L.; Ferrer, J. C.; Maurus, R.; Doran, J.; Carey, P. R.; Brayer, G. D.; Mauk, A. G. *Biochemistry* **1996**, *35*, 11901–11912.
 (36) Hildebrand, D. P.; Tang, H.-I.; Luo, Y.; Hunter, C. L.; Smith, M.; Brayer, G. D.; Mauk, A. G. *J. Am. Chem. Soc.* **1996**, *118*, 12909–12915.
 (37) Shiro, Y.; Iwata, T.; Makino, R.; Fujii, M.; Isoga, Y.; Iizuka, T. *J. Biol. Chem.* **1993**, *268*, 19983–19990.

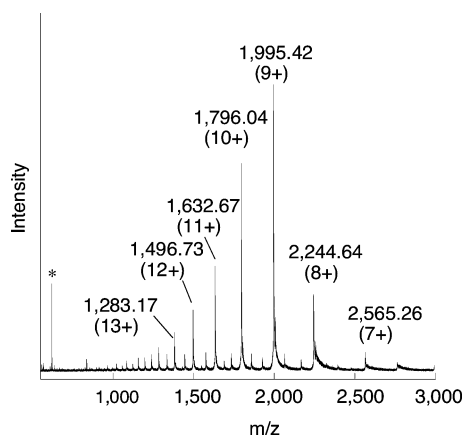


Figure 1. ESI-TOF mass spectrum of wt-rMb(2). The values in parentheses stand for the charge states. The peak with the asterisk(*) is identified as 2 fragmented under the measurement condition.

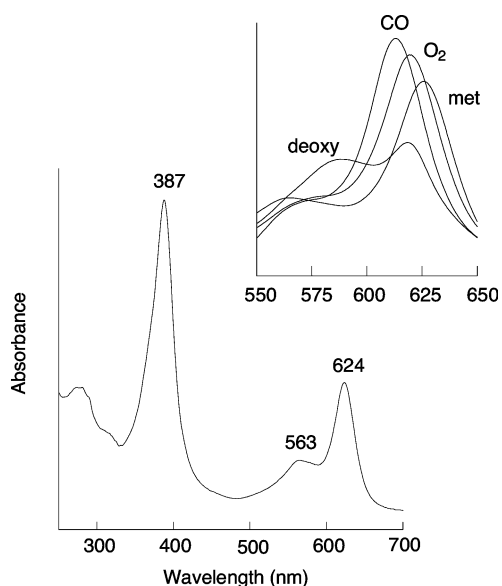


Figure 2. UV-vis spectrum of met-wt-rMb(2); 100 mM phosphate buffer, pH 7.0. Inset: UV-vis spectra of various forms of wt-rMb(2) in the range of wavelengths from 550 to 650 nm.

Table 1. UV-vis Spectral Data for Ferrous wt-rMb(2)^a

sixth ligand	λ_{\max} (nm)
deoxy	352 (sh), 375, 584 (sh), 620
O ₂	387, 562 (sh), 619
CO	391, 567 (sh), 613

^a In 100 mM phosphate buffer, pH 7.0.

On the contrary, in a lower pH region, the UV-vis spectrum of met-wt-rMb(2) changed to that of the free 2, indicating that 2 is dissociated from the protein matrix (Figure 3a). The titration curve shown in Figure 3b affords a pH value corresponding to a 50% dissociation, $pK_{1/2}$. Interestingly, the $pK_{1/2}$ value for wt-rMb(2) is found to be 3.1, which is more acidic than that for wt-Mb(1), by 1.4 pH unit. Figure 3b shows that H64A-rMb(2) also affords almost the same titration curve observed for wt-rMb(2), suggesting that the distal histidine in wt-rMb(2) does not affect the acid denaturation. These results indicate that His93 strongly coordinates to the porphyrine iron in the protein matrix.

Figure 4 shows the EPR spectra of Mbs at 15 K. Both met-wt-rMb(2) and H64A-rMb(2) exhibited only low-spin ($S = 1/2$) signals ($g = 2.43, 2.29,$ and 1.86 for wt-rMb(2) and $g = 2.37, 2.29,$ and 1.89 for H64A-rMb(2)). In contrast, met-wt-Mb(1) and H64A-Mb(1) show the typical high-spin ($S = 5/2$) signals at $g = 6.0$ and 2.0 , which agrees with a previous report.³⁸ Such high-spin and/or spin admixture signals ($S = 5/2$ and $3/2$), as observed for the halogen-coordinated porphyrines,²⁵ were not observed for wt-rMb(2) and H64A-rMb(2). These results suggest that the energy levels of the d-orbitals in rMb(2)s are quite different from those for the Mbs or porphyrines in organic solvents.

The spectroelectrochemical titration of wt-rMb(2) was performed in the presence of anthraquinone-2-sulfonate as an electron mediator. The spectral changes, as shown in Figure 5a, were electrochemically reversible, and the redox potential of Fe(III)/Fe(II) determined from the Nernst plot (Figure 5b) was -190 ± 15 mV vs NHE.³⁹ This value is much lower than the corresponding value for wt-Mb(1) ($+59$ mV vs NHE).⁴⁰ The remarkable difference in the redox potentials between wt-rMb(2) and wt-Mb(1) can be attributed to the lower spin state of wt-rMb(2) with respect to the high spin state of wt-Mb(1).

Ligand Binding for Deoxymyoglobins. The reduction of a ferric rMb with dithionite gave a deoxy-rMb. The deoxy-rMb was subjected to Sephadex G-25 gel chromatography under aerobic conditions to afford a greenish-blue solution ($\lambda_{\max} = 387, 562$ (sh), and 619 nm). When the stream of CO was gently passed into the solution for more than 20 min, the band at 387 nm shifted to 391 nm and the one at 619 nm shifted to 613 nm. Furthermore, passing O₂ gave the solution with the same spectral characteristics again as the above-mentioned greenish solution. From this result, the greenish-blue solution can be identified as the oxy-rMb(2), wt-rMb(2)O₂, and the reversibility between the oxy and CO forms was confirmed. The UV-vis spectral data of these species are summarized in Table 1 and Figure 2 (inset).

The kinetic parameters of the O₂ binding are summarized in Table 2. To evaluate the effects of the distal histidine on the stability of the oxy form, the O₂ bindings for H64A-Mb(1) and H64A-rMb(2) were also measured. The O₂ association rate constant, $k_{\text{on}(O_2)}$, was determined by monitoring the O₂ recombination after cleavage of the Fe-O₂ bond by a laser pulse. From the O₂ association rate constants, it is noted that the reconstitution with 2 enhances the association rate of the O₂ binding by 3–5-fold both in the wild-type and H64A proteins. The O₂ dissociations were measured by the ligand displacement method or ferricyanide oxidation with a stopped-flow apparatus. The observed rate constants at a high concentration of CO or ferricyanide are regarded as the values equal to the O₂ dissociation rate constant, $k_{\text{off}(O_2)}$, because the kinetic profiles show a typical saturation curve against the CO or ferricyanide concentrations.^{10c} However, the oxygenated states of mutant Mbs, H64A-Mb(1) and H64A-rMb(2), were so unstable due to their rapid autoxidations that the conventional methods described above were not available. Therefore, using the double-mixing stopped-flow apparatus, an oxy-Mb was transiently prepared by mixing the corresponding deoxy mutant Mb with O₂-

(38) Egeberg, K. D.; Springer, B. A.; Martinis, S. A.; Sligar, S. G.; Morikis, D.; Champion, P. M. *Biochemistry* **1990**, *29*, 9783–9791.

(39) The reaction of the oxy form, wt-rMb(2)O₂, with dithionite affords the visible spectrum similar to that of the electrochemically reduced state shown in Figure 5a.

(40) Varadarajan, R.; Zewert, T. E.; Gray, H. B.; Boxer, S. G. *Science* **1989**, *243*, 69–72.

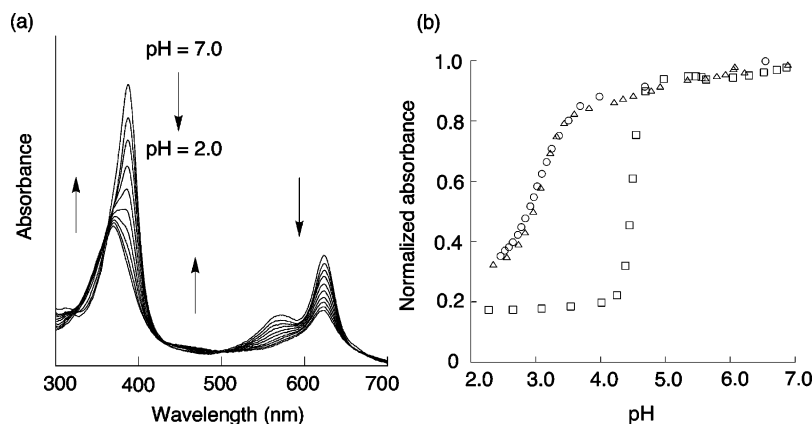


Figure 3. Acid titration for Mbs. (a) Spectral change for wt-rMb(2). (b) Effect of pH on the absorbance at the defined wavelength (normalized by the absorbance at pH 7.0); Δ , wt-rMb(2); \circ , H64A-rMb(2); \square , wt-Mb(1).

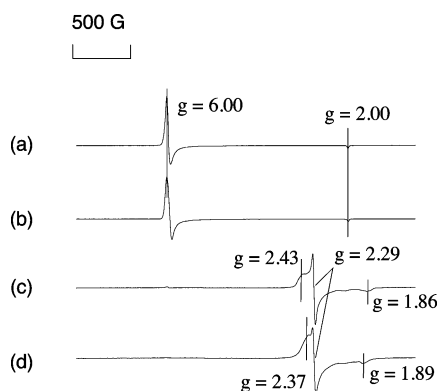


Figure 4. EPR spectra of Mbs: (a) wt-Mb(1), (b) H64A-Mb(1), (c) wt-rMb(2), (d) H64A-rMb(2); 100 mM phosphate buffer, pH 7.0, at 15 K.

saturated buffer, and then CO-saturated buffer was added to the oxy-Mb solution immediately after the aging time of 1.0 s to monitor the displacement of the ligand. The transient spectra after the second mixing with the CO-saturated buffer are shown in Figure 6 (see the Experimental Section for the detailed method for estimating $k_{\text{off}(\text{O}_2)}$).

A series of O_2 dissociation rate constants indicate that the release of O_2 from the reconstituted Mbs dramatically decelerates, compared with those of the corresponding Mbs with the native heme. In addition, interestingly, the O_2 dissociation of H64A-rMb(2) is still lower than that observed in wt-Mb(1), although the former Mb lacks the distal histidine. The rates of autoxidation, an unfavorable process in biological systems, were also measured. For Mbs with the wild-type amino acid residues (wt-Mb(1) and wt-rMb(2)), the first-order decays of the oxygenated species into the corresponding met form gave their autoxidation rates. The mutant Mbs (H64A-Mb(1) and H64A-rMb(2)) also show the rapid disappearance of the oxygenated species with a first-order decay (Figure 7). The autoxidation rates of rMbs in air are also slower than those of the corresponding porphyrin-containing Mbs, suggesting that the oxygenated iron porphycene is more stable than the oxyheme in Mbs.

The O_2 affinities of Mbs were determined from the ratio of the obtained kinetic parameters, $K_{\text{O}_2} = k_{\text{on}(\text{O}_2)}/k_{\text{off}(\text{O}_2)}$. It was found that wt-rMb(2) has a remarkable O_2 affinity 2600-fold higher than that of wt-Mb(1), which is the same tendency as the previous result by horse heart Mbs,³³ as shown in Table 2. Table 2 clearly demonstrates that the enhancement of O_2 affinity

in rMbs mainly stems from the decrease in the dissociation rates, $k_{\text{off}(\text{O}_2)}$. For the H64A mutants, the O_2 affinities of both H64A-Mb(1) and H64A-rMb(2) are much lower than those of the corresponding wild-type Mbs due to the lack of the hydrogen bonding between the bound O_2 and His64. However, H64A-rMb(2) clearly has a higher O_2 affinity than H64A-Mb(1) because of the slow O_2 dissociation from H64A-rMb(2) O_2 . These results indicate that it is not the environment of the distal site but the nature of the porphycene ring mainly contributing to the high O_2 affinities of wt-rMb(2).

The CO binding parameters are summarized in Table 3. The association rates were measured by laser flash photolysis for all of the MbCOs. The obtained rate constants suggest that the CO associations for the reconstituted Mbs are 20–30-fold faster than those observed for Mbs having the native heme.

The dissociation rates for the MbCOs were determined by the ligand displacement with O_2 for wt-rMb(2) or with NO for the other Mbs. In contrast to CO association, it is noteworthy that there is no significant change in the CO dissociation rate upon the replacement of the native heme with the iron porphycene. From these results, it is of particular interest to focus on the O_2/CO discrimination for Mbs. The M' value, the ratio of the CO/ O_2 affinities, yields <1 for wt-rMb(2), whereas the value of wt-Mb(1) is 16 under the same conditions. The remarkable difference is derived from the extremely high O_2 affinity of wt-rMb(2).

Structural Characterization of CO-Bound Forms. To evaluate the structural character of the CO-ligated Mbs, the IR spectra for the C–O stretching modes, $\nu(\text{C–O})$, were collected. The results of the IR measurements for the $\nu(\text{C–O})$ modes are demonstrated in Figure 8. The $\nu(\text{C–O})$ modes of wt-Mb(1)CO were observed at 1932 (minor) and 1945 cm^{-1} (major) and that of H64A-Mb(1)CO at 1965 cm^{-1} , which agrees with the previously reported values.⁴¹ In contrast, the $\nu(\text{C–O})$ bands of the reconstituted Mbs with **2** are broader than that of the corresponding Mbs. These results suggest that there are several electrostatic and/or conformational configurations in rMb(2)-COs.

Discussion

Ferric rMbs. Ferric porphycene **2** was successfully incorporated into apomyoglobin by a conventional method to yield

(41) Li, T.; Quillin, M. L.; Phillips, G. N., Jr.; Olson, J. S. *Biochemistry* **1994**, *33*, 1433–1446.

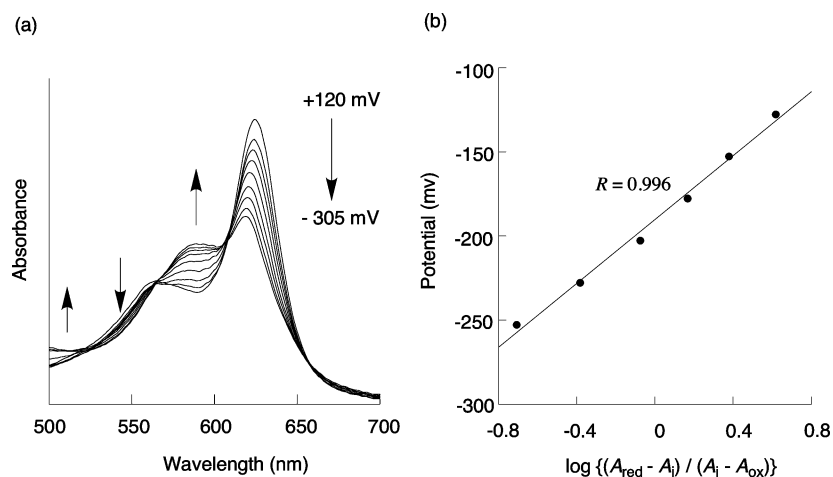


Figure 5. UV-vis spectra of wt-rMb(2) at several applied potentials (versus NHE) during the spectroelectrochemical titration. (a) Overlaid spectra. (b) Nernst plot obtained from the spectral change at 623 nm; 100 mM phosphate buffer, pH 7.0, at 25 °C, under N₂.

Table 2. Kinetic Parameters of O₂ Binding in Mbs^a

Mb	$k_{\text{on}}(\text{O}_2)$ ($\mu\text{M}^{-1}\text{s}^{-1}$) ^b	$k_{\text{off}}(\text{O}_2)$ (s^{-1}) ^c	K_{O_2} (M^{-1}) ^d	k_{auto} (h^{-1}) ^e
wt-rMb(2) ^f	91 ± 10^g	0.057 ± 0.005^h	1.6×10^9	0.024 ± 0.001
wt-Mb(1) ^f	17 ± 1^g	28 ± 2^h	6.1×10^5	0.10 ± 0.01
H64A-rMb(2) ^f	290 ± 20^g	5.9 ± 1.1^h	4.9×10^7	22 ± 3^k
H64A-Mb(1) ^f	90 ± 9^g	5700 ± 500^h	1.6×10^4	87 ± 13^k
hh-rMb(2) ^m	120 ± 10^g	0.11 ± 0.01^h	1.1×10^9	0.026 ± 0.001
hh-Mb(1) ^m	22 ± 1^g	27 ± 2^h	8.1×10^5	0.18 ± 0.01

^a In 100 mM phosphate buffer, pH 7.0. ^b Association rate constants at 25 °C. ^c Dissociation rate constants at 25 °C. ^d $K_{\text{O}_2} = k_{\text{on}}(\text{O}_2)/k_{\text{off}}(\text{O}_2)$. ^e Autoxidation rate constants at 37 °C under atmospheric pressure in air. ^f From sperm whale. ^g Laser flash photolysis under atmospheric pressure in air. ^h Ferricyanide method. ⁱ Laser flash photolysis under 1 atm of CO/O₂ atmosphere (CO/O₂ = 5/95). ^j Double-mixing stopped-flow method was used. ^k Followed the spectral change after mixing deoxy-Mb with 40% O₂-saturated buffer. ^l Laser flash photolysis under 1 atm of O₂. ^m From horse heart (quoted from ref 33).

a reconstituted myoglobin. The UV-vis spectrum of wt-rMb(2) indicates His93 coordination to the porphycene iron. The reversible UV-vis spectral changes between neutral and alkali media suggest that the ferric rMb is an aquomet form under neutral conditions. On the other hand, the spectrum observed at low pH is the same as that of 2-Cl, due to the prosthetic group dissociation from the protein matrix under acidic conditions (pH < 3). The pK_{1/2} value, the pH corresponding to the 50% loss of a prosthetic group, for met-wt-rMb(2) is lower, by 1.4 pH units, than that for met-wt-Mb(1). Furthermore, the pK_{1/2} value for H64A-rMb(2) is consistent with that observed in wt-rMb(2). Because it is known that the pK_{1/2} value is affected by the nature of the Fe-His bond,⁵ the bond strength of Fe-His93 in rMbs seems to be relatively strong for that in wt-Mb(1) and to be independent of the distal structure. This strong coordination of the imidazole to the porphycene iron is also supported by the result of a previous study, where 2,7,17,27-tetra-*n*-propylporphycenatoiron shows a high affinity against the imidazole derivatives in organic solvents.²⁷

According to our EPR studies on met-Mbs, the porphycene iron in wt-rMb(2) shows the typical low-spin character, which is completely different from that observed in wt-Mb(1). In fact, as shown in Figure 4a,b, protohemin 1 with a weakly bound water as the sixth ligand in the protein usually exhibits the high-spin state. Recently, Neya and co-workers reported that the EPR spectrum of the reconstituted Mb with an iron hemiporphycene shows a low-spin character due to the hemichrome conforma-

tion, where the distal histidine (residue 64) coordinates to the iron as well as the proximal histidine.^{21e} Moreover, it is known that a cytochrome *b*₅ with low-spin character has two axially coordinating histidines as the fifth and sixth ligands.⁴² In this regard, the spectrum in Figure 4c, at first glance, suggests that wt-rMb(2) adopts a conformation with a hemichrome-like coordination geometry. However, as shown in Figure 4d, H64A-rMb(2) also has a typical low-spin spectrum despite no distal histidine, indicating the distal histidine in wt-rMb(2) does not coordinate to the iron porphycene, and then, the hemichrome-like conformation should be ruled out. It has been reported that ferric porphycenes coordinated by a halogen atom in organic solvents show high-spin or spin admixture ($S = 5/2$ and $3/2$) signals in their ESR spectra, whereas the corresponding iron porphyrins show high-spin signals.^{25,43} This suggests that an iron atom in a porphycene framework prefers to the lower spin state, compared with the corresponding iron porphyrin. Therefore, the tendency toward the lower spin state of the iron porphycene in organic solvent will be reflected in the spin state of 2 in the myoglobin matrix. The reason for the lower spin state in the porphycene iron is believed to be due to the fact that the smaller cavity formed by the four pyrrole rings with C₂ symmetry destabilizes the d_{x²-y²}-orbital and, in turn, the energy level of d_{x²-y²} is correspondingly lowered.^{25,44} As a result, the d_{x²-y²}-orbital with the highest energy level becomes the unoccupied orbital. To the best of our knowledge, there has been no model study that demonstrated a five-coordinated iron porphycene with an imidazole derivative as an axial ligand. However, it is reasonable that the iron in wt-rMb(2) shows a low-spin character because the proximal imidazole, a stronger field ligand than halides, would bring about the large split in the ligand field, causing a lower spin state in the porphycene iron of the protein.

Although most of the five-coordinated iron porphycenes, which have been reported so far, show similar Fe(III)/Fe(II)

- (42) Rivera, M.; Barillas-Mury, C.; Christensen, K. A.; Little, J. W.; Wells, M. A.; Walker, F. A. *Biochemistry* **1992**, *31*, 12233–12240.
 (43) Some porphyrins, such as [Fe(III)(TPP)(OCIO₃)] and [Fe(III)(OEP)(OCIO₃)], show spin admixture signals ($S = 5/2$ and $3/2$, respectively). (a) Reed, C. A.; Mashiko, T.; Bentley, S. P.; Kastner, M. E.; Scheidt, R. W.; Spartalian, K.; Lang, G. *J. Am. Chem. Soc.* **1979**, *101*, 2948–2958. (b) Masuda, H.; Taga, T.; Osaki, K.; Sugimoto, H.; Yoshida, Z.; Ogoshi, H. *Inorg. Chem.* **1980**, *19*, 950–955.
 (44) Ikeue, T.; Ohgo, Y.; Yamaguchi, T.; Takahashi, M.; Takeda, M.; Nakamura, M. *Angew. Chem., Int. Ed.* **2001**, *113*, 2617–2620.

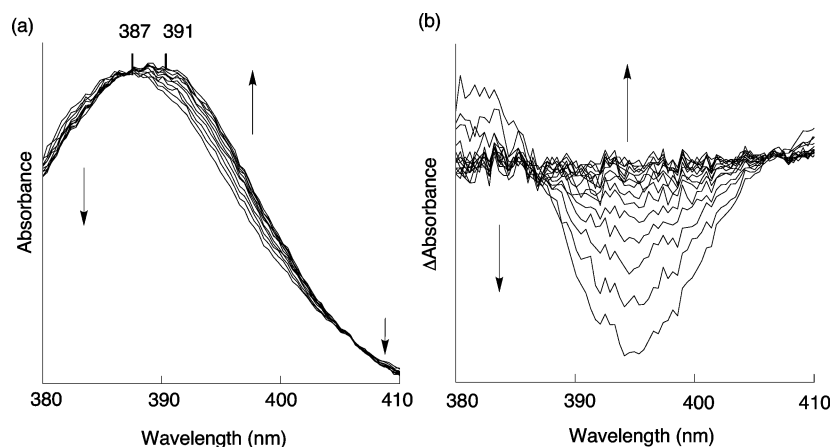


Figure 6. CO replacement of H64A-rMb(2)O₂ with a double-mixing stopped-flow apparatus. (a) Observed spectra after the second mixing, every 0.1 s over 1 s. (b) Differential spectra, every 0.2 s over 3 s. [Mb] = 5.0 μM, 100 mM phosphate buffer, pH 7.0, at 25 °C.

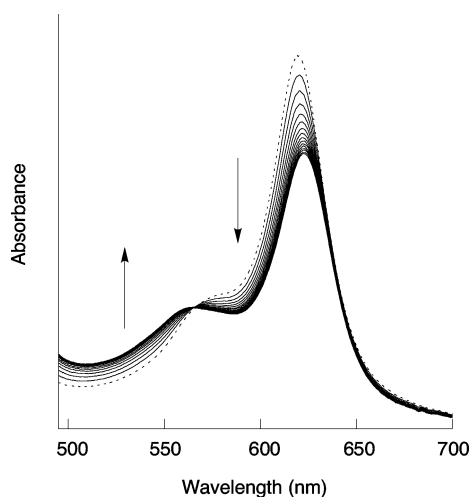


Figure 7. Transient spectra after mixing deoxy-H64A-rMb(2) with 40% O₂-saturated buffer, every 32 s over 480 s. The dotted line is the spectrum collected at $t = 0$; 100 mM phosphate buffer, pH 7.0, at 37 °C.

Table 3. Kinetic Parameters of CO Binding in Mbs^a

Mb	$k_{\text{on}}(\text{CO})$ ($\mu\text{M}^{-1}\text{s}^{-1}$) ^{b,c}	$k_{\text{off}}(\text{CO})$ (s^{-1}) ^d	K_{CO} (M^{-1}) ^e	M' ^f
wt-rMb(2) ^g	11 ± 1	0.070 ± 0.008 ^h	1.6 × 10 ⁸	0.10
wt-Mb(1) ^g	0.51 ± 0.01	0.050 ± 0.006 ⁱ	1.0 × 10 ⁷	16
H64A-rMb(2) ^g	110 ± 11	0.086 ± 0.008 ⁱ	1.3 × 10 ⁹	27
H64A-Mb(1) ^g	3.9 ± 0.4	0.13 ± 0.01 ⁱ	3.0 × 10 ⁷	1900
hh-rMb(2) ^j	13 ± 1	0.031 ± 0.001 ^h	4.2 × 10 ⁸	0.38
hh-Mb(1) ^j	0.61 ± 0.02	0.035 ± 0.002 ⁱ	1.7 × 10 ⁷	21

^a In 100 mM phosphate buffer, pH 7.0. ^b Association rate constants at 25 °C. ^c Laser flash photolysis under 1 atm of CO. ^d Dissociation rate constants at 25 °C. ^e $K_{\text{CO}} = k_{\text{on}}(\text{CO})/k_{\text{off}}(\text{CO})$. ^f $M' = K_{\text{CO}}/K_{\text{O}_2}$. ^g From sperm whale. ^h Replacement with O₂. ⁱ Replacement with NO. ^j From horse heart.

redox potential values to those of the corresponding iron porphyrins,^{23–29} our case is drastically different, where the unusually low redox potential was observed for wt-rMb(2). The unusually low redox potential in wt-rMb(2) can be explained by the spin state of the porphyrine iron in wt-rMb(2). In the case of wt-Mb(1), the electron for reducing the iron can be accommodated in the lowest d-orbital, the d_{xy}-orbital, because the ferric wt-Mb(1) is $S = 5/2$. In contrast, the lowest d-orbital in ferric wt-rMb(2) is completely occupied (due to $S = 1/2$), and then, the additional electron in the reduction process should be accommodated in a higher energy level of the d-orbital (i.e., the d_{yz}- or d_{xz}-orbital). In fact, it has already been reported that

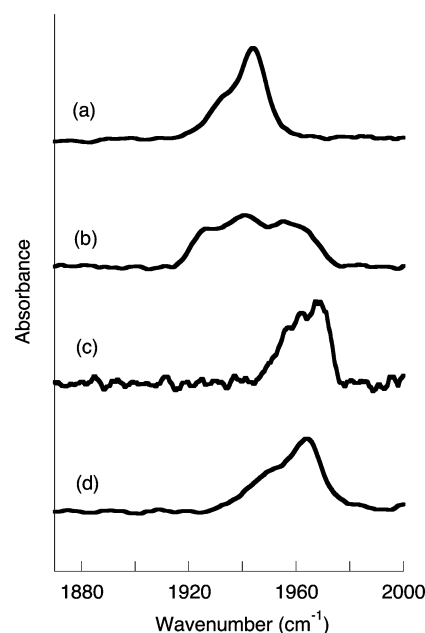


Figure 8. IR spectra of CO-bound Mbs. (a) wt-Mb(1), (b) wt-rMb(2), (c) H64A-Mb(1), (d) H64A-rMb(2); 100 mM phosphate buffer, pH 7.0, at room temperature.

ferric porphyrins with the low-spin state have the tendency of lower oxidation and/or reduction potential(s), although we should note that there is not always a correlation between the redox potential and spin state of the centered metal because some exceptions are known.⁴⁵

O₂ Affinity of rMbs. The most remarkable character of wt-rMb(2) is its extremely high O₂ affinity. It was found that both association and dissociation rates contribute to the enhancement of the O₂ affinity for wt-rMb(2) (~5-fold in $k_{\text{on}}(\text{O}_2)$ and ~1/500-fold in $k_{\text{off}}(\text{O}_2)$). The autoxidation of wt-rMb(2)O₂ is also slower than that of wt-Mb(1)O₂.

Possible factors that contribute to the acceleration of the O₂ association are pointed out as follows. One factor is the structural changes at the distal site upon the reconstitution with an artificial prosthetic group. In fact, it is known that O₂ migration is one of the essential processes affecting $k_{\text{on}}(\text{O}_2)$.⁴⁶ It is reasonable that

- (45) Guillard, R.; Boisselier-Cocolios, B.; Tabard, A.; Cocolios, P.; Simonet, B.; Kadish, K. M. *Inorg. Chem.* **1985**, *24*, 2509–2520.
 (46) Carver, T. E.; Rohlf, R. J.; Olson, J. S.; Gibson, Q. H.; Blackmore, R. S.; Springer, B. A.; Sligar, S. G. *J. Biol. Chem.* **1990**, *265*, 20007–20020.

the porphycene framework and/or the position of the propionate side chains could slightly perturb the protein structure at the distal site, resulting in the easy access of O₂ into the protein matrix. Another reason is the location of the iron atom. This is likely to be the main reason for the acceleration of the O₂ association. In deoxy-Mbs with protoheme IX, the ferrous iron is located out of the porphyrin plane,⁴⁷ and then, the movement of the iron to the in-plane of the porphyrin ring should be accompanied by the process of O₂ association. The out-of-plane positioning of the iron in a deoxy form is caused by the existence of the spin density in the d_{x²-y²}-orbital of the ferrous iron. The d_{x²-y²}-orbital overlaps with the 2p-orbitals of the pyrrole nitrogens to form the Fe-pyrrole nitrogen σ - (and σ^*)-molecular orbitals, and the d_{x²-y²} electron is accommodated in the Fe-pyrrole nitrogen σ^* -orbital in the bond formation. Therefore, the Fe-pyrrole nitrogen bond is somewhat weakened, leading to the iron deviation from the porphyrin plane. On the other hand, the lower symmetry of the porphycene core will destabilize the d_{x²-y²} level, resulting in the fact that the d_{x²-y²}-orbital of a relatively high energy level would be vacant. As a result, the iron is positioned in the plane of the porphycene.^{48,49} Therefore, O₂ can readily bind to the porphycene iron without the movement of the iron.

The kinetic data clearly indicate that the extremely high O₂ affinity in wt-rMb(2) is predominantly caused by the very slow O₂ dissociation. One of the factors to characterize the oxy-Mb is the Fe–O₂ bond configuration, and both σ -bond and π -bond characters are considered.³⁰ The former bonding mode is suggested by the Fe–O–O bond angle,⁶ and the latter mode is proposed by some spectroscopic studies of oxy-Mbs^{7,8} or by ligand binding of Mb model compounds.^{30–32} The retardation of the O₂ dissociation on wt-rMb(2) is accounted for by the effect of the porphycene framework on the energy levels of the d-orbitals in the porphycene iron. As described above, the energy level of the d_{z²}-orbital of the porphycene iron is stabilized in wt-rMb(2) due to the lower symmetry of the porphycene framework. The decrease in the energy level of the d_{z²}-orbital allows a stable Fe–O₂ σ -bond with energetically favorable overlap of the d_{z²}-orbital with a π^* -orbital of O₂ to form. It has already been reported that the arrangement of four pyrroles leads to the stabilization of the Fe–O₂ σ -bond, contributing to the deceleration of the O₂ dissociation.^{21e} Therefore, the stable Fe–O₂ σ -bonding is likely to be the main factor of the slow O₂ dissociation in rMb(2)s.

On the other hand, it could be argued that the Fe–O₂ π -bonding mode is also important for the slow O₂ dissociation of wt-rMb(2) because the Mb model compound studies have suggested that the coordination of an axial ligand to the centered iron promotes the Fe–O₂ π -bonding character, and the strong coordination of His93 in wt-rMb(2) could facilitate Fe–O₂ π -bonding, leading to Fe^{δ+}–O–O^{δ-} charge separation. In this case, the interaction between the imidazole proton on His64 and O₂ may be close to a charge-dipole interaction by the increase in electron density on O₂, resulting in the tightening

of the hydrogen bonding between O₂ and distal His in the rMb(2)O₂s. Although it is difficult to directly evaluate the strength of the hydrogen bonding between His64 and the bound O₂ in the rMb(2)s, we compared the O₂ binding behavior of the wild-type Mbs with that of the H64A mutants in order to investigate, in detail, the effect of this hydrogen bonding on O₂ dissociation and the contribution of the Fe–O₂ π -bonding mode in the oxy-rMb(2)s. If the argument described above was valid, the O₂ dissociation rate of H64A-rMb(2)O₂ should be almost the same or faster than that of wt-rMb(2)O₂. The results of the kinetic measurements indicated that the dissociation of O₂ is accelerated in about the same ratio in both H64A-rMb(2)O₂ and H64A-Mb(1)O₂ due to truncation of the distal histidine. However, the O₂ dissociation rate constant for H64A-rMb(2)O₂ is 1/100 smaller than that for H64A-Mb(1)O₂. Thus, it should be concluded that although the hydrogen bonding between O₂ and His64 is essential for holding O₂ in the rMbs, the special enhancement in the hydrogen bonding interaction between His64 and O₂ does not occur in wt-rMb(2).

The kinetic parameters of the autoxidation from oxy-Mb to met-Mb also give an insight into the stability of oxy-Mb because the correlation between the O₂ affinities and autoxidation rates has been reported in a series of wild-type and mutant Mbs.⁵⁰ It was found that wt-rMb(2)O₂ has a slower autoxidation rate than that of wt-Mb(1)O₂. In contrast, the autoxidation rate of H64A-rMb(2)O₂ is 22-fold faster than that of wt-Mb(1) and is accelerated by 2 orders of magnitude, compared with that of wt-rMb(2)O₂. These are attributed to the effect of truncation of the hydrogen bonding at the distal site. When a set of H64A-Mbs (H64A-rMb(2) and H64A-Mb(1)) is compared, the autoxidation of the former is 1/4 that of the latter. The tendency in the autoxidation rate constants agrees with the relationship between the autoxidation rate constants and O₂ dissociation described above.⁵¹

CO Affinity of rMbs. The CO affinities for rMbs are also enhanced by the replacement of the native heme with iron porphycene 2. Table 3 shows that the enhancement of the CO affinity is mainly caused by the acceleration of the CO association, although an extremely high O₂ affinity is derived from the slow O₂ dissociation. The large acceleration of CO association in rMbs can be also explained by the in-plane location of the porphycene iron because it is known that the Fe–CO bond formation is more essential to the association rate of CO than the migration from the outside of the protein.⁴⁶

On the other hand, the CO dissociation rates of the rMbs are almost the same as those of the corresponding porphyrin-containing Mbs. The rate for H64A-rMb(2) is slightly slower than that for H64A-Mb(1), but the difference is not significant. In contrast, Figure 8 shows that the IR spectrum of wt-rMb(2)CO is remarkably different from that observed in wt-Mb(1)CO. The C–O stretching band of wt-rMb(2)CO displays an overlap of several bands in the range of frequencies from 1930–1970 cm⁻¹. This character is also observed in H64A-rMb(2). These spectra with several C–O stretching suggest that there are several electronic and/or structural conformers for the Fe–

(47) Kachalova, G. S.; Popov, A. N.; Bartunik, H. D. *Science* **1999**, *284*, 473–476.

(48) In the X-ray structure of ferrous four-coordinated tetrapropylporphycene, the iron is located in the ring plane (see ref 26).

(49) According to the quantum chemical calculation on an iron porphycene coordinated by an imidazole molecule, the in-plane location of the iron is energetically favored. Nakashima, H.; Hasegawa, J.; Nakatsuji, H. Private communication.

(50) Brantley, R. E., Jr.; Smerdon, S. J.; Wilkinson, A. J.; Singleton, E. W.; Olson, J. S. *J. Biol. Chem.* **1993**, *268*, 6995–7010.

(51) The autoxidation rate is affected by the concentration of O₂ and has the maximum value when the concentration of O₂ is equal to 1/K_{O₂} (see ref 50). The 1/K_{O₂} value for wt-rMb(2) is much smaller than the concentration of O₂ under 1 atm of air.

Table 4. Kinetic Parameters of O₂ Binding in Myoglobins and *Ascaris* Hb

protein	$k_{\text{on(O}_2\text{)}}\text{ (}\mu\text{M}^{-1}\text{s}^{-1}\text{)}$	$k_{\text{off(O}_2\text{)}}\text{ (s}^{-1}\text{)}$	$K_{\text{O}_2}\text{ (M}^{-1}\text{)}$
wt-Mb(1) ^a	17 ± 1	28 ± 2	6.1 × 10 ⁵
wt-rMb(2) ^a	91 ± 10	0.057 ± 0.005	1.6 × 10 ⁹
<i>Ascaris</i> Hb ^b	1.5	0.004	3.8 × 10 ⁸

^a From this work. ^b From ref 12a.

C–O bond⁵² in the rMb(2)s as well as the native protein;⁴¹ however, the broadening is outstanding in wt-rMb(2). According to the previous report, the C–O stretching frequencies are affected by the electrostatic interactions between amino acid residues at the distal site and the CO group.⁴¹ For example, the hydrogen bonding between the amino acid residue and the terminal oxygen in the CO group induces a decrease in the C–O stretching frequency, whereas the C–O stretching modes for mutants lacking such amino acid residues that can form hydrogen bonding are observed in a higher wavenumber than that of the wild-type.⁴¹ The broad C–O stretching band is supposed to be caused by the existence of several configurations in the interactions between the amino acid residues and the CO group. However, there was no observation of a multicomponent decay in the CO dissociation kinetics for the rMbCOs. One possible reason is that the apparent dissociation rate is an average of the values for these conformers; otherwise, they are in rapid equilibrium.^{41,52} Since the C–O stretching band for wt-rMb(2)CO is widely distributed both in lower and higher wavenumbers, compared with that for wt-Mb(1)CO, the dissociation rate constant of wt-rMb(2)CO may be apparently similar to that of wt-Mb(1)CO, as observed in this study. Although the origin of the multiple Fe–C–O bond configurations in wt-rMb(2)CO is not clearly known at the moment, we propose the following two factors. First, the lower frequencies are due to the enhancement of π -back-donation from the iron to π^* -orbitals of CO. The coordination of the proximal histidine may affect the π -back-donation from the iron to π^* -orbitals of CO.^{30–32} Second, as another possible factor, the slight structural changes of the distal site due to the possession of an artificial prosthetic group could bring out the structural disorder of the distal histidine, adopting multiple orientations with both strong and weak interactions with the bound ligand. A more-precise discussion on the Fe–C–O bond configuration will be done in future.⁵³

Unusual O₂ Selectivity against CO. As the result of the extremely high O₂ affinity of wt-rMb(2) with iron porphycene 2, the M' values of these Mbs are less than 1, that is to say, their O₂ affinities are *greater* than the CO affinities. The similar O₂/CO discrimination is also observed in some native proteins, such as *Ascaris* Hb, although they have protoheme IX as a prosthetic group. Therefore, it is of interest to compare the kinetic parameters of ligand binding between wt-rMb(2) and *Ascaris* Hb to reveal the sharp contrast in the mechanism of the ligand bindings between them.

The kinetic parameters of the O₂ and CO binding for these proteins are summarized in Tables 4 and 5. Both the O₂ and

Table 5. Kinetic Parameters of CO Binding in Myoglobins and *Ascaris* Hb

protein	$k_{\text{on(CO)}}\text{ (}\mu\text{M}^{-1}\text{s}^{-1}\text{)}$	$k_{\text{off(CO)}}\text{ (s}^{-1}\text{)}$	$K_{\text{CO}}\text{ (M}^{-1}\text{)}$	M' ^a
wt-Mb(1) ^b	0.51 ± 0.01	0.050 ± 0.006	1.0 × 10 ⁷	16
wt-rMb(2) ^b	11 ± 1	0.070 ± 0.008	1.6 × 10 ⁸	0.10
<i>Ascaris</i> Hb ^c	0.17–0.21	0.018	(0.94–1.2) × 10 ⁷	0.02–0.032

^a $M' = K_{\text{CO}}/K_{\text{O}_2}$. ^b From this work. ^c From ref 12a.

CO association rates for wt-rMb(2) are much faster than those of *Ascaris* Hb (80-fold for $k_{\text{on(O}_2\text{)}}$ and 60-fold for $k_{\text{on(CO)}}$) In deoxy-wt-rMb(2), the iron is in-plane of the porphycene, resulting in acceleration of the ligand associations. The resonance Raman spectrum for $\nu(\text{Fe-proximal His})$ in deoxy-*Ascaris* Hb suggests that the iron of this protein is also located in the plane of the porphyrin framework.^{10b} However, there are bulky amino acid residues, such as Tyr and Gln, at the distal site in *Ascaris* Hb.¹² Therefore, this would make a ligand migration harder for *Ascaris* Hb.

On the other hand, the O₂ dissociation of wt-rMb(2) and *Ascaris* Hb are much slower than that of wt-Mb(1). The 3D structure of the oxygenated *Ascaris* Hb shows that the systematic hydrogen bonding network at the distal site stabilizes the O₂ on the heme to slow the O₂ dissociation.^{12c} In contrast, the small $k_{\text{off(O}_2\text{)}}$ for wt-rMb(2) is due to the stabilization of the Fe–O₂ σ -bond interaction. Thus, it should be noted that the ligand binding mechanism is quite different between wt-rMb(2) and *Ascaris* Hb, although both proteins show a remarkably high O₂ affinity. *Ascaris* Hb achieves high O₂ affinity by the environment of the distal site, whereas in wt-rMb(2), the nature of the prosthetic group contributes to both the O₂ association and the dissociation.

Ascaris Hb decelerates the CO dissociation, whereas the rate for wt-rMb(2) is almost the same as that determined in the wt-Mb(1). This finding is attributed to the existence of hydrogen bondings between the terminal oxygen of CO and Tyr30 or Gln64 in the same manner as the oxy form. This can account for the small CO dissociation rate in *Ascaris* Hb.¹² On the other hand, wt-rMb(2) has only His64 as a hydrogen bonding donor for CO molecule. As a result, the apparent CO dissociation rate for wt-rMb(2) can be similar to that of the wild-type Mb.

Conclusion

We successfully prepared the reconstituted Mb with a remarkably high O₂ affinity and unusual and characteristic O₂/CO discrimination using the iron porphycene as a prosthetic group without any point mutations at the distal site. To the best of our knowledge, this work demonstrates the most drastic enhancement of O₂ affinity among the studies on Mb modification ever reported. The high O₂ affinities in the rMb(2)s are predominantly due to the nature of the porphycene ring, not the effect of the environment in the protein matrix. The low symmetry of porphycene framework allows the formation of the stable Fe–O₂ σ -bond, leading to the slower O₂ dissociation rate. The intrinsically larger stability of the Fe–O₂ bond in wt-rMb(2) is also supported by the smaller M' value of H64A-rMb(2) than that of H64A-Mb(1), where we do not need to consider the influence of the distal imidazole on the bond configuration. The difference between porphyrin and porphycene is also reflected in the very unique physicochemical properties of the ferric rMb(2)s. In general, it is difficult to characterize

(52) Das, T. K.; Friedman, J. M.; Kloek, A. P.; Goldberg, D. E.; Rousseau, D. L. *Biochemistry* **2000**, *39*, 837–842.

(53) As preliminary data, the resonance Raman spectra for the rMb(2)COs also show the broad bands for the Fe–CO stretching modes. The data agree with the results of the IR measurements.

the monoimidazole-ligated ferric and ferrous porphycenes and oxygenated species in organic solutions. The present work is regarded as the first example to monitor these species by use of the protein matrix. Thus, apo-Mb is a good tool for understanding the chemical properties of new metalloporphyrins and their analogues and provides us with a unique approach in the field of coordination chemistry. On the other hand, the present results indicate that the reconstitution with an artificial prosthetic group is a powerful method to dramatically modulate the protein function. This method, called "chemical mutation", by a synthetic prosthetic group will serve as the technique to produce tailor-made proteins with a variety of functions.

Acknowledgment. We express our gratitude to Professor Teizo Kitagawa, Dr. Shigenori Nagatomo (Center of Integrative Bioscience, Okazaki, Japan), Professor Yoshinori Naruta, and

Dr. Fumito Tani (Kyushu University, Japan) for helping to collect the resonance Raman spectra. We acknowledge Professor Hiroshi Nakatsuji, Dr. Jun-ya Hasegawa, and Mr. Hiroyuki Nakashima (Kyoto University, Japan) for helpful discussions on theoretical aspects of an iron porphycene. We appreciate the assistance of Ms. Midori Watanabe at the Center of Advanced Instrumental Analysis (Kyushu University) for the IR measurements. We thank Mr. Hideki Horiuchi (Kyushu University) for his skillful glassblowing. Finally, we are grateful for the financial support by the Japan Science and Technology Agency (JST), the Japan Society for the Promotion of Science (JSPS), and the Ministry of Education, Culture, Sports, Science and Technology, Japan. This work was also supported in part by Kato Memorial Bioscience Foundation.

JA045880M